
[View Journal Online](#)  
[View Article Online](#)

# Crystal structure, in silico molecular docking, DFT analysis and ADMET studies of *N*-(2-methoxy-benzyl)-acetamide

Suganya Murugan <sup>1</sup>, Prasanth Gunasekaran <sup>2</sup>, Jayasudha Nehru <sup>1</sup>, Anaglit Catherine Paul <sup>1</sup>, Necmi Dege <sup>3</sup>, Emine Berrin Cinar <sup>3</sup>, Savaridasson Jose Kavitha <sup>1</sup>, Kasthuri Balasubramani <sup>4</sup>, Kaliyaperumal Thanigaimani <sup>5</sup>, Venkatachalam Rajakannan <sup>2</sup> and Madhukar Hemamalini <sup>1,\*</sup>

<sup>1</sup> Department of Chemistry, Faculty of Science, Mother Teresa Women's University, Kodaikanal, 624101, India

<sup>2</sup> Centre of Advanced Study in Crystallography and Biophysics, Faculty of Science, University of Madras, Chennai, 600025, India

<sup>3</sup> Department of Physics, Faculty of Science, Ondokuz Mayıs University, Samsun, 55200, Turkey

<sup>4</sup> Department of Chemistry, Faculty of Science, Government Arts College (Autonomous), Thanthonimalai, Karur, 639005, India

<sup>5</sup> Department of Chemistry, Faculty of Science, Government Arts College, Trichy, 620022, India

\* Corresponding author at: Department of Chemistry, Faculty of Science, Mother Teresa Women's University, Kodaikanal, 624101, India.

e-mail: [hemamalini2k3@yahoo.com](mailto:hemamalini2k3@yahoo.com) (M. Hemamalini).

## RESEARCH ARTICLE

## ABSTRACT



doi: 10.5155/eurjchem.13.4.440-450.2303

Received: 08 July 2022

Received in revised form: 01 September 2022

Accepted: 09 September 2022

Published online: 31 December 2022

Printed: 31 December 2022

## KEYWORDS

PARP protein  
 Crystal structure  
 Molecular docking  
 Density functional theory  
 Hirshfeld surface analysis  
 Molecular electrostatic potential

In this work, *N*-(2-methoxy-benzyl)-acetamide (2MBA) was synthesized from an amide derivative and it was characterized by FT-IR and NMR spectroscopy techniques. The crystal structure of 2MBA was also validated via single-crystal X-ray diffraction analysis. Crystal data for C<sub>10</sub>H<sub>13</sub>NO<sub>2</sub> for 2MBA: Monoclinic, space group *P*2<sub>1</sub>/*n* (no. 14), *a* = 9.1264(6) Å, *b* = 9.3375(7) Å, *c* = 11.9385(8) Å, β = 95.745(5)°, *V* = 1012.26(12) Å<sup>3</sup>, *Z* = 4, μ(MoKα) = 0.082 mm<sup>-1</sup>, *D*<sub>calc</sub> = 1.176 g/cm<sup>3</sup>, 5632 reflections measured (5.368° ≤ 2θ ≤ 51.992°), 1990 unique (*R*<sub>int</sub> = 0.0377, *R*<sub>sigma</sub> = 0.0314) which were used in all calculations. The final *R*<sub>1</sub> was 0.0583 (*I* > 2σ(*I*)) and *wR*<sub>2</sub> was 0.1444 (all data). The intermolecular interactions in 2MBA were theoretically examined by Hirshfeld surface analysis and 2D fingerprint plots. Moreover, the HOMO and LUMO energy gaps of 2MBA was calculated by DFT calculation with the B3LYP/6-311G++(d,p) method. The electron-withdrawing and donating sites of the 2MBA were confirmed via molecular electrostatic potential surface analysis. The present study discusses the title compound not only highlighted the crystallographic data but also revealed good molecular interactions together with an anticancer drug target, which is a targeting PARP protein, which was an important drug target in the treatment of breast cancer.

Cite this: *Eur. J. Chem.* 2022, 13(4), 440-450

Journal website: [www.eurjchem.com](http://www.eurjchem.com)

## 1. Introduction

Medicinal chemistry plays an important role in the development of drugs for curing, maintaining, and improving the health of humans. The significance of the amidation reactions (C=O with N-H), including peptide bond-forming reactions, is one of the most fundamental transformations in organic chemistry and the pharmaceutical industry. The rising costs of waste disposal have prompted researchers to look for new methods for amide bond formation that avoid the formation of unwanted materials while increasing atom economy [1-3]. Recent literature studies revealed that acetamide and various amide derivatives showed many biological activities such as antifungal, antibacterial, antioxidant, anticancer, anti-inflammatory, anti-arthritis, anticancer, and anthelmintic activities [4-7]. Numerous acetamide derivatives have been reported to be active as antimicrobial agents [8].

To explore the effect of the 2MBA compound on breast cancer, we use the molecular docking methodology for the

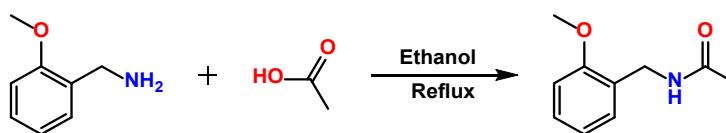
evaluation of molecular-level interactions with the important class of drug targets in breast cancer treatment [9]. The ADMET properties [10] and the effect of the amide compound against cancer were predicted using Swiss ADME and Way2Drug servers [11], and the molecular docking of the 2MBA compound with drug targets was carried out through Autodock Tools 4.2 [12]. 2MBA was docked with a total of four drug targets PARP1, PARP2, Tankyrase 1, and Tankyrase 2, belonging to the PARP protein family [13]. The results are compared with data on drugs, olaparib and talazoparib, which are available for treatment to inhibit molecular targets [14]. This work explains crystallization, structure refinement, Hirshfeld surface analysis, density functional theory calculations, and molecular docking as an important study on the 2MBA compound [15].

## 2. Experimental

### 2.1. Instrumentation

**Table 1.** Crystal data and structure refinement parameters for 2MBA.

Empirical formula	C <sub>10</sub> H <sub>13</sub> NO <sub>2</sub>
Formula weight	179.21
Temperature (K)	296(2)
Crystal system	Monoclinic
Space group	P2 <sub>1</sub> /n
a, (Å)	9.1264(6)
b, (Å)	9.3375(7)
c, (Å)	11.9385(8)
β (°)	95.745(5)
Volume (Å <sup>3</sup> )	1012.26(12)
Z	4
ρ <sub>calc</sub> (g/cm <sup>3</sup> )	1.176
μ (mm <sup>-1</sup> )	0.082
F(000)	384.0
Crystal size (mm <sup>3</sup> )	0.78 × 0.657 × 0.48
Radiation	MoKα (λ = 0.71073)
2θ range for data collection (°)	5.368 to 51.992
Index ranges	-11 ≤ h ≤ 11, -11 ≤ k ≤ 11, -14 ≤ l ≤ 13
Reflections collected	5632
Independent reflections	1990 [R <sub>int</sub> = 0.0377, R <sub>sigma</sub> = 0.0314]
Data/restraints/parameters	1990/0/120
Goodness-of-fit on F <sup>2</sup>	1.073
Final R indexes [I ≥ 2σ (I)]	R <sub>1</sub> = 0.0583, wR <sub>2</sub> = 0.1304
Final R indexes [all data]	R <sub>1</sub> = 0.0870, wR <sub>2</sub> = 0.1444
Largest diff. peak/hole (e.Å <sup>-3</sup> )	0.16/-0.17
CCDC Number	2145614

**Scheme 1.** Synthesis of *N*-(2-methoxy-benzyl)-acetamide (2MBA).

The FT-IR spectrum was recorded in a FTIR Perking Elmer Spectrum400 spectrophotometer using the KBr pellet method. The solution state <sup>1</sup>H NMR and <sup>13</sup>C NMR spectrum were recorded on a Bruker Advance III HD Nanobay 400 MHz FT-NMR spectrometer. The sample was analyzed in deuterated DMSO and the chemical shifts were relative to tetramethylsilane (TMS) as reference [16,17].

## 2.2. Synthesis of *N*-(2-methoxy-benzyl)-acetamide (2MBA)

All the chemicals and solvents used in this investigation were of analytical reagent grade. 2-Methoxy-benzylamine and acetic acid were purchased from Merck and were used without further purification. 2-Methoxy-benzylamine (1 mmol, 0.0343 g) and acetic acid (1 mmol, 0.0150 g) were dissolved in 25 mL of ethanol and the solution mixture was heated very slowly and refluxed for 6 h with constant stirring. The reaction mixture was then cooled to room temperature and the obtained precipitate was filtered [15]. The precipitate was recrystallized with ethanol. Finally, the acquired product *N*-(2-methoxy-benzyl)-acetamide is shown in Scheme 1.

*N*-(2-Methoxy-benzyl)-acetamide (2MBA): Color: White/needle shape. Yield: 76%. M.p.: 80-85 °C. FT-IR (KBr, ν, cm<sup>-1</sup>): 1603 (C=O), 3015 (C-H), 3289 (N-H). <sup>1</sup>H NMR (400 MHz, DMSO-*d*<sub>6</sub>, δ, ppm): 1.02 (s, 3H, CH<sub>3</sub>), 3.79 (s, 3H, O-CH<sub>3</sub>), 4.20 (s, 2H, CH<sub>2</sub>), 6.90 (t, 1H, Ar-H), 6.96 (d, 1H, Ar-H), 7.10 (d, 1H, Ar-H), 7.22 (t, 1H, Ar-H), 8.08 (s, 1H, NH). <sup>13</sup>C NMR (100 MHz, DMSO-*d*<sub>6</sub>, δ, ppm): 176.70, 157.02, 128.34, 127.68, 127.49, 120.57, 110.87, 37.28, 34.43, 20.11.

## 2.3. Single crystal structure determination

Single crystal X-ray diffraction analysis was carried out on STOE IPDS diffractometer using a MoKα radiation (λ = 0.71073 Å) at 296(2) K. The softwares used for crystal structure analysis: to data collection, APEX3 [18]; to cell refinement and data reduction, SAINT [19]; to solve the structure, SHELXS-97

[20,21], to refine the structure, SHELXL-97 [20,21], to molecular graphics and publication material, OLEX2 [22] and ORTEP3 [23]. The crystal data and structure refinement parameter details are given in Table 1. All H atoms were positioned geometrically (N-H = 0.86 Å and C-H = 0.93-0.97 Å were refined using a riding model, with *U*<sub>iso</sub>(H) = 1.2 or 1.5*U*<sub>eq</sub>(C, O).

## 2.4. Hirshfeld surface analysis

To analyze the intermolecular interactions in the crystal structure, Hirshfeld surfaces were mapped with *d*<sub>norm</sub>, and their associated 2D fingerprint was plotted using Crystal Explorer 17.5 [24].

## 2.5. Computational study

Theoretical calculations were obtained by density functional theory (DFT) with the B3LYP/6-311G++(d,p) basis set using the Gaussian 09W program [25]. Additionally, the HOMO-LUMO energies and molecular electrostatic potential were calculated with the same level of theory. In silico ADME screening using the SwissADME website (<http://www.swissadme.ch/index.php>) to evaluate individual ADME behavior, such as physicochemical properties, lipophilicity, water solubility, pharmacokinetics, drug likeness and BOILED Egg properties of 2MBA [26-29]. The biological activity of the title compound was predicted using the free online webserver WAY2DRUG (<http://www.way2drug.com/index.php>) to predict the effect of the compound against different biological assays [11]. From the results of predicted biological activity, the breast cancer target proteins were selected for molecular docking and the title compound was docked with Poly (ADP-Ribose) polymerases (PARP), a group of potential drug targets in cancer therapy [30]. The crystal structures of important PARP class proteins such as PARP-1 (PDB: 7KK2), PARP-2 (PDB: 4TVJ), Tankyrase-1 (PDB: 7KKM), Tankyrase-2 (PDB: 3KR7) were downloaded from the RCSB database [13,14].

**Table 2.** Bond lengths (Å) and bond angles (°) for 2MBA.

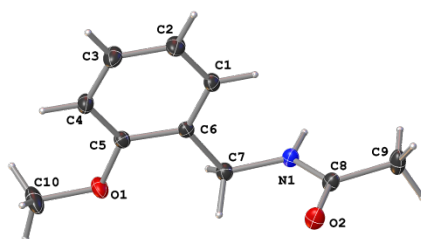
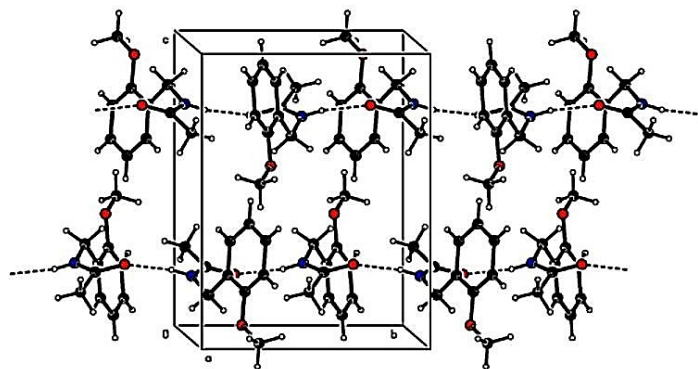
Atom	Atom	Length		Atom	Atom	Length	
		X-ray	DFT			X-ray	DFT
O1	C5	1.366(2)	1.374	C6	C7	1.510(3)	1.514
O1	C10	1.419(3)	1.423	C5	C4	1.373(3)	1.394
O2	C8	1.231(2)	1.222	C8	C9	1.496(3)	1.519
N1	C8	1.324(3)	1.365	C1	C2	1.382(3)	1.396
N1	C7	1.441(3)	1.460	C4	C3	1.381(3)	1.397
C6	C5	1.387(3)	1.407	C2	C3	1.363(4)	1.388
C6	C1	1.376(3)	1.391				

Atom	Atom	Atom	Angle		Atom	Atom	Atom	Angle	
			X-ray	DFT				X-ray	DFT
C5	O1	C10	117.51(19)	118.65	O2	C8	N1	122.4(2)	123.06
C8	N1	C7	122.99(17)	122.77	O2	C8	C9	121.7(2)	121.50
C5	C6	C7	118.98(17)	120.15	N1	C8	C9	115.94(19)	115.42
C1	C6	C5	118.02(18)	118.02	C6	C1	C2	121.2(2)	121.43
C1	C6	C7	122.99(18)	121.43	N1	C7	C6	114.75(17)	113.43
O1	C5	C6	115.08(18)	115.32	C5	C4	C3	119.3(2)	119.55
O1	C5	C4	123.62(19)	123.92	C3	C2	C1	119.6(2)	119.35
C4	C5	C6	121.29(19)	120.74	C2	C3	C4	120.5(2)	120.50

**Table 3.** Hydrogen bond interaction of the title compound.

D-H...A	d(D-H), Å	d(H...A), Å	d(D...A), Å	∠D-H...A, °	Symmetry
N1-H1A...O2	0.86	1.99	2.836(2)	169.1	3/2-x, -1/2+y, 1/2-z

**Figure 1.** The asymmetric unit of *N*-(2-methoxy-benzyl)-acetamide.**Figure 2.** The package of *N*-(2-methoxy-benzyl)-acetamide.

AUTODOCK TOOLS 4.2 software [12] was used for molecular docking and the grid box parameters was adjusted in the active site residues of protein targets and the results were analyzed [31] and compared with the co-crystal structures of the olaparib and talazoparib drugs [13,14] using PyMol [32], Ligplot [33] and Poseview [34,35].

### 3. Results and discussion

#### 3.1. Single crystal structure analysis

The ORTEP view of 2MBA is shown in Figure 1 with a dihedral angle of 86.18(13)° between the benzene ring and the mean plane of the carboxamide group C-C(O)-N. The N1-C8, C8-O2, and C8-C9 bond lengths are 1.324(3), 1.231(2), and 1.496(3) Å, respectively (Table 2). The C8-O2 bond distance in the amide group shows a partial double-bond character and is similar in length to those found in the crystal structure of the 3-

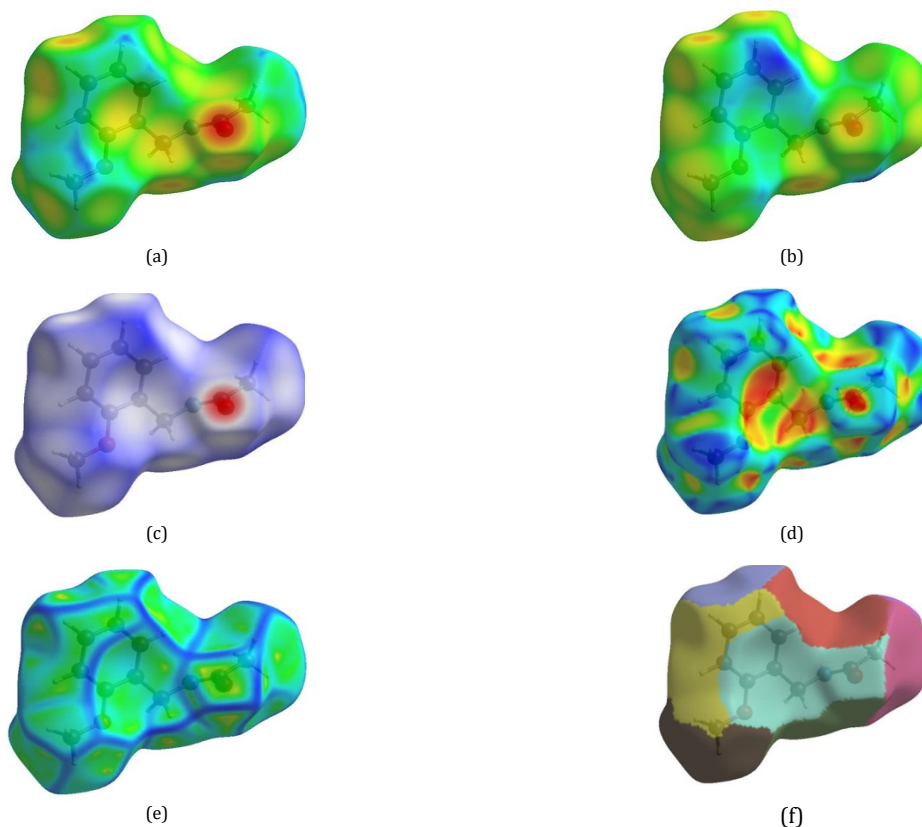
acetoxy-2-methyl-*N*-(4-nitrophenyl) benzamide, (1.215(2) Å [36]. The benzene ring, C1-C2-C3-C4-C5-C6, is planar with an RMS deviation of -0.004(2) Å at C1. The torsion angles of C7-N1-C8-O2 and C7-N1-C8-C9 -0.1(3) and -179.6(2)° compared with theoretical values of -4.15 and 176.4°, respectively. From the theoretical values, it was found that calculated values of bond length and bond angles slightly difference from the experimental values, by the DFT-B3LYP/6-311G++(d,p) basis set as shown in Table 2. In the crystal structure, neighboring molecules are linked by strong N1-H1A...O2 hydrogen bonds (3/2-x, -1/2+y, 1/2-z), forming supramolecular chains along the *b*-axis direction (Figure 2 and Table 3).

#### 3.2. Hirshfeld surface analysis

The Hirshfeld surface (HS) analysis provides qualitative and quantitative details about intermolecular close contacts in molecular crystals.

**Table 4.** Energy values of 2MBA.

Color	N	Symp	R	Electron density	$E_{ele}$	$E_{pol}$	$E_{dis}$	$E_{rep}$	$E_{tot}$
Red	2	$x+1/2, -y+1/2, z+1/2$	7.49	B3LYP/6-31G(d,p)	-4.2	-1.9	-11.0	7.7	-10.6
Orange	2	$x, y, z$	9.13	B3LYP/6-31G(d,p)	-6.3	-2.1	-11.3	5.5	-14.7
Yellow	2	$-x+1/2, y+1/2, -z+1/2$	6.64	B3LYP/6-31G(d,p)	-1.0	-1.1	-17.8	5.8	-13.7
Green	2	$x+1/2, -y+1/2, z+1/2$	8.19	B3LYP/6-31G(d,p)	-4.3	-1.7	-12.7	5.6	-13.4
Cyan	1	$-x, -y, -z$	6.50	B3LYP/6-31G(d,p)	-0.7	-0.9	-18.7	7.1	-13.3
Blue	1	$-x, -y, -z$	6.37	B3LYP/6-31G(d,p)	-0.3	-1.1	-19.3	9.1	-12.3
Purple	2	$-x+1/2, y+1/2, -z+1/2$	6.42	B3LYP/6-31G(d,p)	-43.3	-11.4	-24.2	49.7	-44.6
Pink	1	$-x, -y, -z$	11.56	B3LYP/6-31G(d,p)	-1.1	-0.1	-1.8	0.2	-2.6

**Figure 3.** (a) Hirshfeld surface plots over  $d_e$ , (b)  $d_i$ , (c)  $d_{norm}$ , (d) Shape index, (e) Curvedness and (f) Fragment patch.

The distances can be defined as  $d_e$  (distance from the nearest nucleus inside to the surface) and  $d_i$  (distance from the nearest nucleus outside to the surface) as shown in Figures 3a and 3b. The  $d_{norm}$  surface shown in Figure 3c (range of -0.5942 to 1.5253 a.u.) represents a red spot of intensity and shows the presence of dominant interactions. Figure 3d shows the shape index map produced within the range -1 to 1 Å. The convex blue portions indicate hydrogen donor groups, while the concave red parts represent hydrogen acceptor groups. The nonexistence of contiguous red and blue triangles on the shape-index plot indicates the absence of  $\pi$ - $\pi$  interactions. The curvedness map, generated in the range -4.0 to 4.0 Å, as shown in Figure 3e, depicts enormous areas of green with no flat (i.e., planar) surface area, while the blue patches show areas of curvature. The fragment patch plot ranging from 0 to 13.0000 a.u. provides the neighbor coordination environment based on the color of the patch shown in Figure 3f. The overall two-dimensional fingerprint (FPs) with the largest contacts of H...H interaction contributes 61.6% to the surface, followed by C...H/H...C contacts at 18.9% which are important contributors to structural stability via hydrogen bonding, O...H/H...O contacts at 18.1%, and the shortest contacts of N...H/H...N interaction at 1.4% shown in Figure 4.

The total interaction energy is obtained by the combination of the electrostatic energy  $E_{ele}$ , the exchange repulsion energy  $E_{rep}$ , the polarization energy  $E_{pol}$ , and the dispersion

energy  $E_{dis}$  were performed by the CE-B3LYP/6-31G(d,p) method. In Table 4, the highest interaction energy  $E_{tot} = -44.6$  kJ/mol (shown by purple color) from the centroid of the selected 2MBA associated with symmetry operation  $(-x+1/2, y+1/2, -z+1/2)$  and the molecular distance  $R = 6.42$  Å. Whereas the lowest interaction energy  $E_{tot} = -2.6$  kJ/mol (shown by pink color) with the symmetry code  $(-x, -y, -z)$  and the molecular distance  $R = 11.56$  Å (Figure 5) [37]. The  $E_{tot}$  for the intermolecular interaction N1-H1A...O2 is  $169.1^\circ$  (Table 3).

### 3.3. DFT studies

The quantum chemical calculations of 2MBA have been performed by DFT/B3LYP/6-311G++(d,p) basis set, using the Gaussian 09W program [25]. The optimized molecular structure is shown in Figure 6 and the related geometrical parameters are given in Table 2.

#### 3.3.1. Frontier molecular orbitals

Frontier molecular orbitals (FMOs), the highest occupied molecular orbital (HOMO), and the lowest unoccupied molecular orbital (LUMO) are the most significant parameters for quantum chemistry, electrical properties, and molecule interactions with other species.

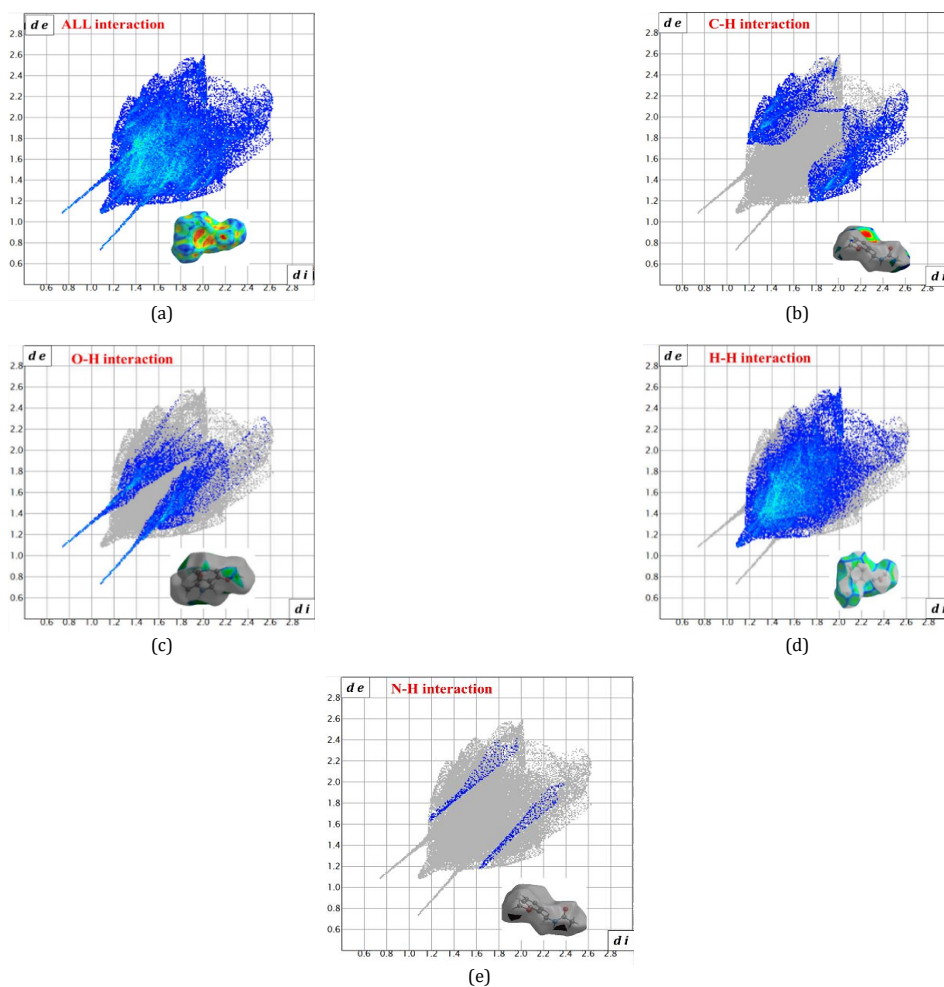


**Figure 4.** Two-dimensional fingerprint plot for the title compound showing the contributions of individual types of interactions: (a) all intermolecular contacts, (b) C $\cdots$ H contacts, (c) O $\cdots$ H/H $\cdots$ O contacts, (d) H $\cdots$ H contacts, and (e) N $\cdots$ H/H $\cdots$ N contacts.

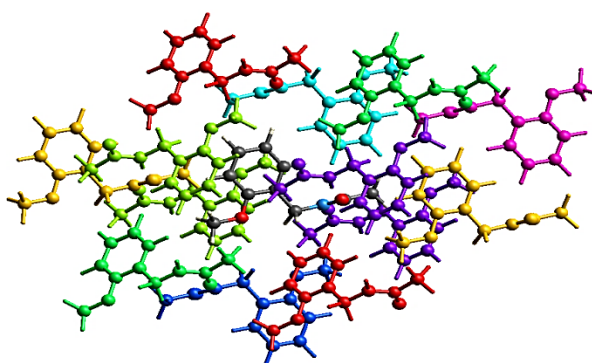


**Figure 5.** Energy frameworks of 2MBA.

The chemical reactivity descriptors [38] such as  $E_{\text{HOMO}}$  ionization potential (A),  $E_{\text{LUMO}}$  electron affinity, chemical hardness ( $\eta$ ), chemical potential ( $\mu$ ), softness (S), electronegativity ( $\chi$ ), nucleophilicity index ( $\epsilon$ ) and electrophilicity index ( $\omega$ ) of the 2MBA molecule shown in Table 5. The energy gap for 2MBA is 5.7795 eV. Therefore, the molecule is highly polarizable and highly reactive (Figure 7).

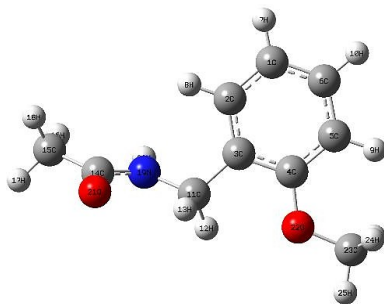
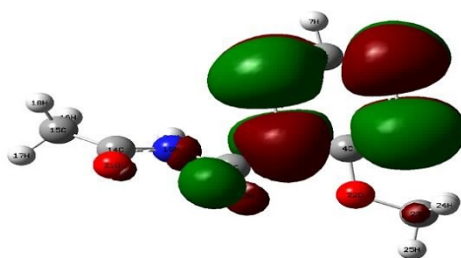
### 3.3.2. Molecular electrostatic potential

The molecular electrostatic potential (MEP) map is an important tool for explaining the electrostatic interactions. In

order to find the most active regions of the molecule, the molecular electrostatic potential map surfaces were taken into consideration. The negative area, which is considered a nucleophilic site, is usually colored red (the strongest repulsion), whereas the positive region, which is the preferred electrophilic site, is colored blue (the strongest attraction). The green-colored patch on the map shows a neutral potential. From the MEP map as shown in Figure 8, it is evident that most of the reactive and negative region is around the methoxy group. The electrons present in this area could be readily provided to the acceptor species [39].

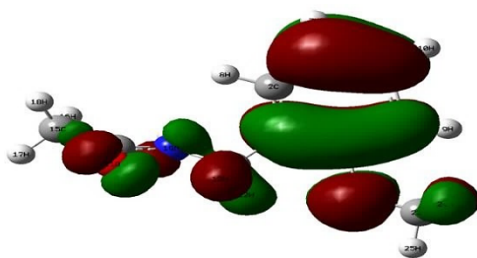
**Table 5.** Calculated frontier molecular orbital analysis and chemical reactivity descriptors of the 2MBA.

Parameters	Equations	Values
$E_{\text{HOMO}}$	HOMO	-6.4014
$E_{\text{LUMO}}$	LUMO	-0.6219
$I$	Minus of HOMO	6.4014 eV
$A$	Minus of LUMO	0.62190 eV
$E_{\text{gap}}$	$\Delta E = (I-A)$	5.7795 eV
Chemical hardness	$\eta = (I-A)/2]$	2.88975 eV
Chemical potential	$\mu = -(I+A)/2)$	3.51165 eV
Electronegativity	$\chi = (-\mu)$	-3.51165eV
Softness	$S = (1/\eta)$	0.34605 1/eV
Electrophilicity index	$\omega = (\mu^2/2\eta)$	2.1337 eV
Nucleophilicity index	$\varepsilon = 1/\omega$	0.4687 eV
Dipole moment	$\mu$	5.2885

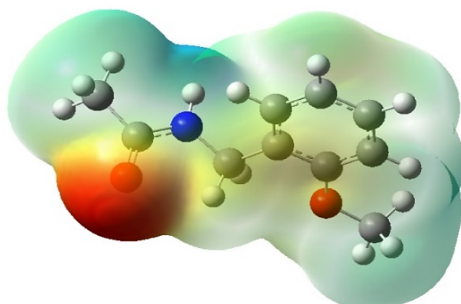
**Figure 6.** DFT optimized structure of 2MBA.

$$E_{\text{LUMO}} = -0.6219 \text{ eV}$$

$$\downarrow E_{\text{gap}} = 5.7795 \text{ eV}$$



$$E_{\text{HOMO}} = -6.4014 \text{ eV}$$

**Figure 7.** The graphical presentation of the HOMO-LUMO of 2MBA.**Figure 8.** The MEP surfaces of 2MBA by using DFT/B3LYP/6311G++(d,p).

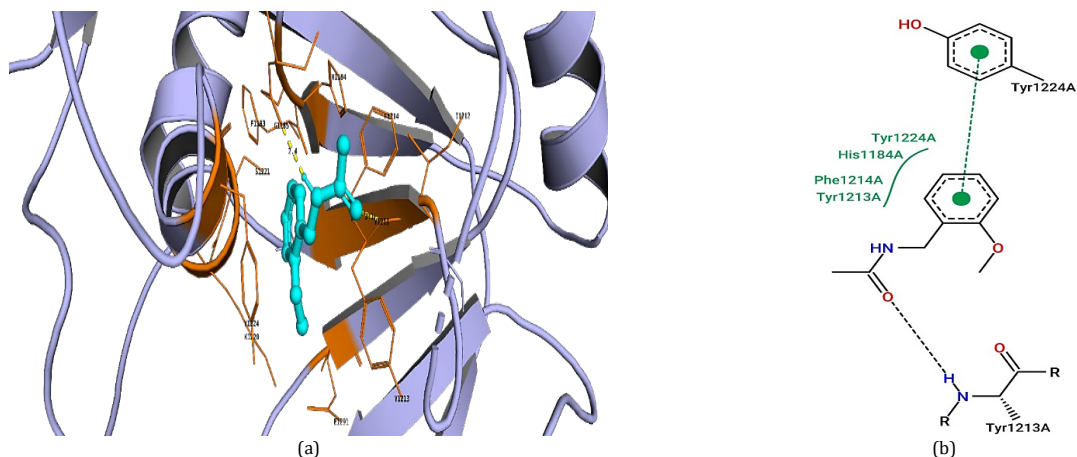


**Figure 9.** Molecular interaction analysis of ligand with Tankyrase-1. (a) Three-dimensional representation of molecular interaction of title compound with tankyrase-1 (PDB: 7KKM) (Tankyrase-1: cartoon pale blue, hydrogen, and hydrophobic interacting residues: orange lines, ligand: cyan stick) and (b) Two-dimensional representation of molecular interaction of title compound with Tankyrase-1 (PDB: 7KKM) active site residues. (Dotted line-hydrogen bonds, arc structures-residues involved in hydrophobic interaction).

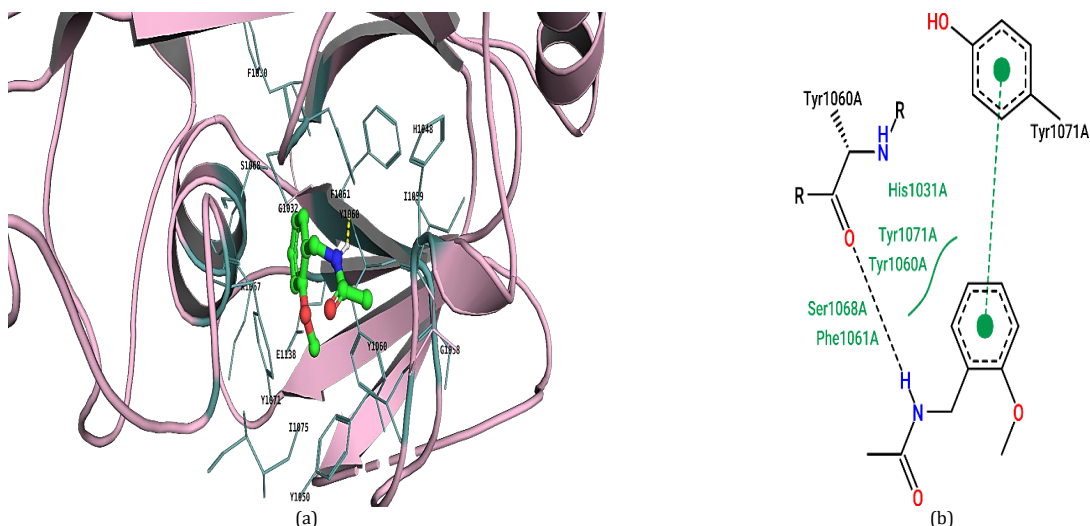


**Figure 10.** Molecular interaction analysis of ligand with Tankyrase-2. (a) Three-dimensional representation of molecular interaction of title compound with Tankyrase-2 (PDB: 3KR7) and (b) Two-dimensional representation of molecular interaction of title compound with Tankyrase-2 (PDB: 3KR7) active site residues. (Dotted line-hydrogen bonds, arc structures-residues involved in hydrophobic interaction).

### 3.4. Molecular docking

The *in-silico* analysis of the cell line activity of the title compound using the Way2Drug server shows maximum activity toward the MDA-MB-453 cell line belonging to breast adenocarcinoma (Table 6). The 2MBA molecule was analyzed for PARP protein inhibition activity through molecular docking; the function of the PARP protein was to play an important role in the single-strand DNA repair mechanism, where it binds with NAD<sup>+</sup> to produce ADP-ribose-monomers. PARP (Poly ADP ribose polymerase) inhibitors were an important class of medications used in the treatment of advanced or metastatic breast cancer with individuals having HER2-negative BRCA gene mutations [40-42]. The docking results of 2MBA with the PARP protein exhibit better interactions with the catalytic site residues of Tankyrase-1 and Tankyrase-2. The 2MBA/Tankyrase-2 complex has a binding energy of -6.27 kcal/mol, which was the least binding energy compared to the Tankyrase-1, PARP-1, and PARP-2 complexes. 2MBA has hydrogen bonding with one of the catalytic residues TYR1060 and hydrophobic interaction with the other two catalytic residues (HIS 1031, Glu 1138), and one  $\pi$ - $\pi$  interaction with the ring of TYR 1071 of Tankyrase-2 protein. Like Tankyrase-2, the 2MBA has two hydrogen bonds with catalytic residue TYR1213, and the

other hydrogen bond interaction is with residue GLY 1185 (Figure 9-11). There is no interaction observed with the catalytic residues of PARP-1 protein and the 2MBA interacts only through hydrophobic interaction with two catalytic residues of PARP-2 protein (Tables 7 and 8).

### 3.5. Swiss ADME studies

The values of physicochemical properties of 2MBA molecule show have a polar surface area of 38.33 Å<sup>2</sup> with 50.52 refractive indexes and fraction Csp3 (Table 9). The lipophilicity analysis of the 2MBA molecule shows a consensus Log P<sub>o/w</sub> value of 1.48 which shows that it passes one of the important ADMET properties. The three different solubility index calculations show a moderate solubility character in water. The pharmacokinetic properties of the title compound show high gastrointestinal absorption with no observed P-glycoprotein binding affinity and the blood-brain barrier crossing property with all cytochrome P isoform inhibition properties. The amide 2MBA shows no violation against Lipinski's rule, GOSE rule, VEBER rule, EGAN, and MUEGGE rule, which indicated its good drug likeliness properties with a bioavailability score of 0.55 [29].

**Table 6.** 2MBA activity against the cell lines predicted by the Way2Drug server.

Pa*	Pi*	Cell line	Cell line full name	Tissue	Tumor type
0.443	0.034	MDA-MB-453	Breast adenocarcinoma	Breast	Adenocarcinoma
0.372	0.087	NALM-6	Adult B acute lymphoblastic leukemia	Hematopoietic and lymphoid tissue	Leukemia
0.341	0.079	U-266	Plasma cell myeloma	Blood	Myeloma
0.378	0.135	Hs 683	Oligodendroglioma	Brain	Glioma
0.332	0.104	CFPAC-1	Pancreatic carcinoma	Pancreas	Carcinoma
0.258	0.085	LS174T	Colon adeno carcinoma	Colon	Adenocarcinoma
0.260	0.092	MKN-7	Gastric carcinoma	Stomach	Carcinoma
0.179	0.021	U2OS	Osteosarcoma	Bone	Sarcoma
0.245	0.087	CCRF-CEM	Childhood T acute lymphoblastic leukemia	Blood	Leukemia
0.263	0.136	HOS	Osteosarcoma	Bone	Sarcoma
0.248	0.123	HOP-18	Non-small cell lung carcinoma	Lung	Carcinoma
0.158	0.035	SK-BR-3	Breast adenocarcinoma	Breast	Adenocarcinoma
0.249	0.128	NCI-H1299	Non-small cell lung carcinoma	Lung	Carcinoma
0.198	0.077	Ovarian carcinoma cells	Ovarian adenocarcinoma	Ovary	Adenocarcinoma
0.109	0.017	MOLT-3	T-lymphoblastic leukemia	Blood	Leukemia
0.133	0.044	D54	Glioblastoma	Brain	Glioblastoma
0.091	0.020	JAM	Ovarian cystadenocarcinoma	Ovary	Adenocarcinoma
0.157	0.090	Jurkat	Acute leukemic T-cells	Blood	Leukemia
0.095	0.028	KETR3	Renal carcinoma	Kidney	Carcinoma
0.086	0.020	DO4	Melanoma	Skin	Melanoma
0.136	0.074	SH-SY5Y	Bone marrow neuroblastoma	Brain	Neuroblastoma
0.211	0.153	NCI-H69	Small cell lung carcinoma	Lung	Carcinoma
0.120	0.062	NSCLC	Non-small cell lung carcinoma	Lung	Carcinoma
0.064	0.020	UMUC3	Bladder carcinoma	Urinary tract	Carcinoma
0.233	0.195	MCF7	Breast carcinoma	Breast	Carcinoma
0.223	0.187	Hs-578T	Invasive ductal breast carcinoma	Breast	Carcinoma
0.128	0.094	LXFL 529	Non-small cell lung carcinoma	Lung	Carcinoma
0.057	0.028	CEM-SS	Childhood T acute lymphoblastic leukemia	Blood	Leukemia
0.027	0.005	NT2	Embryonal carcinoma	Germ cell. Fibroblast	Carcinoma
0.063	0.050	SW1353	Bone chondrosarcoma	Bone	Sarcoma
0.052	0.039	TCC-SUP	Bladder carcinoma	Urinary tract	Carcinoma
0.101	0.089	MeWo	Melanoma	Skin	Melanoma
0.081	0.075	DAN-G	Human pancreas adenocarcinoma cell line	Pancreas	Adenocarcinoma
0.056	0.050	UMSCC22B	Hypopharyngeal squamous cell carcinoma	Upper aerodigestive tract	Carcinoma
0.138	0.133	MAXF401	Breast carcinoma	Breast	Carcinoma
0.176	0.171	M19-MEL	Melanoma	Skin	Melanoma
0.030	0.026	BE-NQ	Colon adenocarcinoma	Colon	Adenocarcinoma
0.024	0.023	C180-13S	Ovarian carcinoma	Ovary	Carcinoma
0.207	0.206	PC-6	Small cell lung carcinoma	Lung	Carcinoma

**Table 7.** Protein target details, grid box parameters and molecular docking results.

PDB ID	Name	Grid box coordinates (x, y, z)	Grid box size (x, y, z)	Binding energy (kcal/mol)	Inhibition constant ( $\mu$ M)	Intermolecular energy (kcal/mol)	VDW desolv. energy (kcal/mol)
3KR7	Tankyrase-2	9.736, 3.712, 12.826	22, 40, 42	-6.27	25.27	-7.17	-7.12
7KKM	Tankyrase-1	1.207, 8.131, 19.136	40, 44, 36	-5.99	40.88	-6.88	-6.81
7KK2	PARP-1	-6.923, 3.070, 9.444	50, 40, 50	-5.67	69.76	-6.57	-6.24
4TVJ	PARP-2	20.389, 0.872, 22.411	58, 32, 40	-5.19	155.61	-6.09	-6.01

**Table 8.** Information about the hydrogen, hydrophobic interaction, and pi-pi interaction.

Name	Hydrogen bonds	Hydrophobic interaction	Pi-Pi interaction
Tankyrase-2	Tyr 1060	Lys1067, His1048, Phe1030, Glu1138, Gly1032, Ser1068, Phe1061, Ala1062, Tyr1060, His1031, Gly1058	Tyr1071
Tankyrase-1	Tyr 1213, Gly 1185	Lys1220, Glu1291, Phe1214, Ala1215, Ser1221, His1184, Ser1186.	Tyr1224
PARP-1	Arg 878, Asp 770	Tyr710, Pro 881, Leu769, Ala880, Asp766, Ile879, Ile872, Leu877	-
PARP-2	Gly 429	Tyr462, Glu558, His428, Ser470, Ala464, Ser430	Tyr473

**Table 9.** Physico-chemical properties of 2MBA

Physicochemical properties	Lipophilicity	Water solubility	Pharmacokinetics
Formula	C <sub>10</sub> H <sub>13</sub> NO <sub>2</sub>	Log Po/w (iLOGP)	GI absorption
Molecular weight, g/mol	179.22	Log Po/w (XLOGP3)	High
Num. heavy atoms	13	Log Po/w (WLOGP)	BBB permeant
Num. arom. heavy atoms	6	Log Po/w (MLOGP)	Yes
Fraction Csp <sup>3</sup>	0.30	Log S (Ali)	P-gp substrate
Num. rotatable bonds	4	Log S (SILICOS-IT)	No
Num. H-bond acceptors	2	Consensus Log Po/w	Yes
Num. H-bond donors	1	Log S (SILICOS-IT)	CYP1A2 inhibitor
Molar Refractivity	50.52	Solubility	CYP2C9 inhibitor
TPSA	38.33 Å <sup>2</sup>	Solubility	No
		Class	CYP2D6 inhibitor
		Class	CYP3A4 inhibitor
		Class	Log Kp (skin permeation)
		Class	-6.59 cm/s

The nil alertness in PAINS and BRENK rule with a synthetic accessibility score of 1.13 shows a possible drug-likeness property of 2MBA. Bioavailability radar of the molecule (Figure 12a) prepared from the SWISSADME server. The pink area represents the optimal range for each property such as lipophilicity (XLOGP3 -0.7 to +5.0), Molecular weight (150 to 500 g/mol), polarity: TPSA (20 to 130 Å<sup>2</sup>), solubility (Log S not more than 6), saturation (fraction of carbons in the *sp*<sup>3</sup> hybridization not less than 0.25), and flexibility (no more than

9 rotatable bonds). Here, our molecule values cover an optimal area of all properties showing good drug likeliness character. BOILED-EGG (WLOGP vs TPSA) plot of 2MBA is given in Figure 12b. The red dot structure shows that 2MBA is not an inhibitor of P-glycoprotein, and its presence inside the yellow yolk region explains its high penetration capability of the blood-brain barrier. The future work will focus on altering the molecule character to improve the water solubility with less cytochrome P isoforms inhibition.

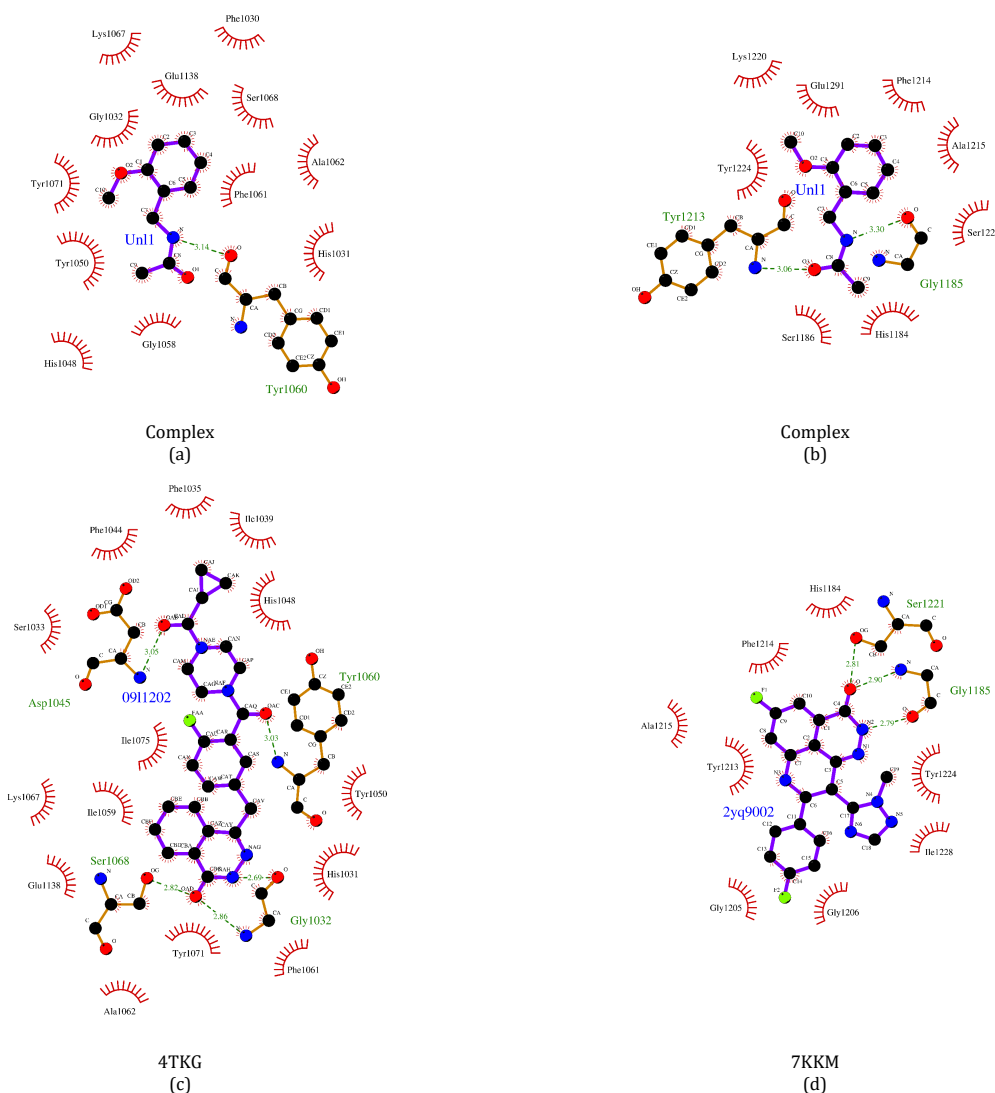


**Figure 11.** Molecular interactions of the ligand with Tankyrase-1 and Tankyrase-2 compared with molecular interactions of drugs olaparib and talazoparib complexed crystal structure. (a) Hydrogen and hydrophobic interaction plot generated using LIGPLOT for the title ligand docked with Tankyrase-2 (PDB: 3KR7) (Dotted line-hydrogen bonds, arc structures-residues), (b) Hydrogen and hydrophobic interaction plot generated using LIGPLOT for the ligand docked with Tankyrase-1, (PDB: 7KKM) (Dotted line-hydrogen bonds, arc structures-residues), (c) Hydrogen and hydrophobic interaction plot generated using LIGPLOT for drug olaparib with Tankyrase-2 crystal structure downloaded from RCSB (PDB: 4TKG) (Dotted line-hydrogen bonds, arc structures-residues involved in hydrophobic interaction), (d) Hydrogen and hydrophobic interaction plot generated using LIGPLOT for drug talazoparib with Tankyrase-1 crystal structure downloaded from RCSB (PDB: 7KKM) (Dotted line-hydrogen bonds, arc structures-residues involved in hydrophobic interaction).

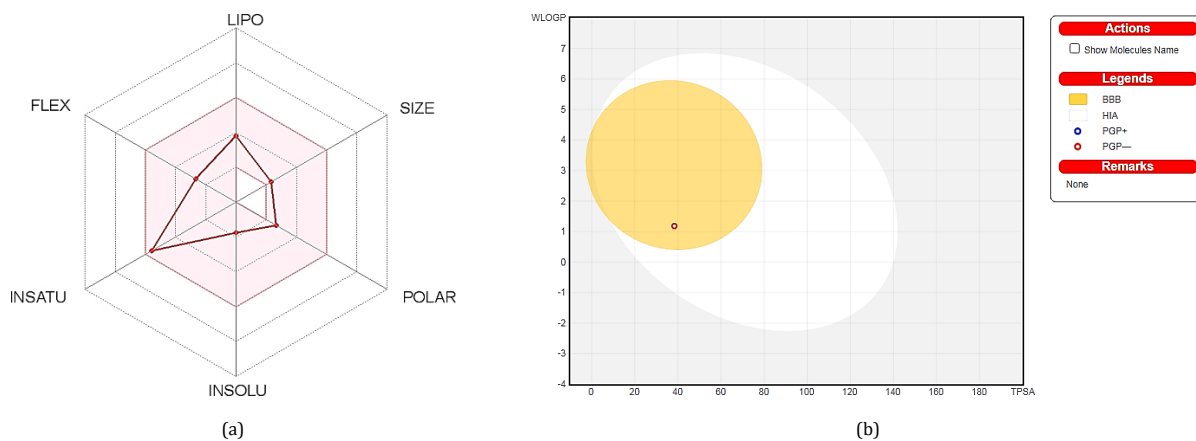


**Figure 12.** (a) Bioavailability radar and (b) BOILED-EGG plot of 2MBA.

#### 4. Conclusions

In the present work, *N*-(2-methoxy-benzyl)acetamide derived from 2-methoxybenzylamine and acetic acid was successfully synthesized. The obtained compound was characterized by using spectroscopic analysis, such as FT-IR and NMR studies. Our findings also characterize the FMO and MEP concepts that were successfully applied in 2MBA to confirm the experimental results. Non-covalent supramolecular interactions in the crystal structure were quantified through Hirshfeld  $d_{norm}$  surfaces and 2D fingerprint plots to predict the percentage interactions. The quantum chemical parameters such as chemical hardness, softness electronegativity, HOMO-LUMO energy gap,  $E_{LUMO}$ , and  $E_{HOMO}$  provide important clues about the biological activity of the amide 2MBA have been calculated with the B3LYP/6-311G++(d,p) method. In addition, a positive result of kinase inhibition was implicated by a molecular docking study against anticancer activity. Furthermore, drug-likeness and pharmacodynamics data revealed that 2MBA completed ADME requirements and has good drug score values. The molecular docking results show the interaction of compounds like olaparib and talazoparib drug compounds and the interaction of the compound with Tankyrase-1 and Tankyrase-2 has been potential evidence to proceed the further studies on the compound for future cancer-based activity.

#### Acknowledgments

Madhukar Hemamalini thanks the Science and Engineering Research Board Science, International Research Experience (SERB-IRE) for financial support; Ref. No. SIR/2022/000011. Anaglit Catherine Paul thanks Mother Teresa Women's University, Tamil Nadu, India, for financial support.

#### Supporting information

CCDC-2145614 contains the supplementary crystallographic data for this paper. These data can be obtained free of charge via [www.ccdc.cam.ac.uk/data\\_request/cif](http://www.ccdc.cam.ac.uk/data_request/cif), or by e-mailing [data\\_request@ccdc.cam.ac.uk](mailto:data_request@ccdc.cam.ac.uk), or by contacting The Cambridge Crystallographic Data Centre, 12 Union Road, Cambridge CB2 1EZ, UK; fax: +44(0)1223-336033.

#### Disclosure statement

Conflict of interest: The authors declare that they have no conflict of interest. Ethical approval: All ethical guidelines have been adhered. Sample availability: Sample of the 2MBA is available from the author.

#### CRedit authorship contribution statement

Conceptualization: Madhukar Hemamalini; Methodology: Suganya Murugan, Jayasudha Nehru; Software: Venkatachalam Rajakannan, Prasanth Gunasekaran, Necmi Dege, Emine Berrin Cinar; Validation: Madhukar Hemamalini, Venkatachalam Rajakannan, Savaridasson Jose Kavitha; Formal Analysis: Suganya Murugan, Anaglit Catherine Paul, Jayasudha Nehru; Investigation: Kaliyaperumal Thanigaimani; Resources: Madhukar Hemamalini; Data Curation: Necmi Dege, Emine Berrin Cinar; Writing - Original Draft: Madhukar Hemamalini, Suganya Murugan; Writing - Review and Editing: Savaridasson Jose Kavitha, Madhukar Hemamalini; Visualization: Suganya Murugan, Anaglit Catherine Paul; Funding acquisition: Madhukar Hemamalini, Anaglit Catherine Paul; Supervision: Madhukar Hemamalini; Project Administration: Madhukar Hemamalini.

#### ORCID and Email

Suganya Murugan

 [sugan.chemists@gmail.com](mailto:sugan.chemists@gmail.com)

 <https://orcid.org/0000-0001-9707-9998>

Prasanth Gunasekaran

 [prasanthbiophysics@gmail.com](mailto:prasanthbiophysics@gmail.com)

 <https://orcid.org/0000-0001-9996-2960>

Jayasudha Nehru

 [sujijaya145@gmail.com](mailto:sujijaya145@gmail.com)

 <https://orcid.org/0000-0003-4694-5328>

Anaglit Catherine Paul

 [acatherine.paul@gmail.com](mailto:acatherine.paul@gmail.com)

 <https://orcid.org/0000-0002-5217-1616>

Necmi Dege

 [necmid@omu.edu.tr](mailto:necmid@omu.edu.tr)

 <https://orcid.org/0000-0003-0660-4721>

Emine Berrin Cinar

 [emineberrin.cinar@omu.edu.tr](mailto:emineberrin.cinar@omu.edu.tr)

 <https://orcid.org/0000-0001-7617-3459>

Savaridasson Jose Kavitha

 [josekavitha@gmail.com](mailto:josekavitha@gmail.com)

 <https://orcid.org/0000-0002-6513-2210>

Kasthuri Balasubramani

 [manavaibala@gmail.com](mailto:manavaibala@gmail.com)

 <https://orcid.org/0000-0003-1724-9999>

Kaliyaperumal Thanigaimani

 [thanigaimani81@gmail.com](mailto:thanigaimani81@gmail.com)

 <https://orcid.org/0000-0002-4384-7848>

Venkatachalam Rajakannan

 [vrajakannan@gmail.com](mailto:vrajakannan@gmail.com)

 <https://orcid.org/0000-0002-4129-9227>

Madhukar Hemamalini

 [hemamalini2k3@yahoo.com](mailto:hemamalini2k3@yahoo.com)

 [hemamalini.ch@motherteresawomensuniv.ac.in](mailto:hemamalini.ch@motherteresawomensuniv.ac.in)

 <https://orcid.org/0000-0001-8233-9451>

#### References

- Humphrey, J. M.; Chamberlin, A. R. Chemical synthesis of natural product peptides: Coupling methods for the incorporation of noncoded amino acids into peptides. *Chem. Rev.* **1997**, *97*, 2243–2266.
- Ghose, A. K.; Viswanadhan, V. N.; Wendoloski, J. J. A knowledge-based approach in designing combinatorial or medicinal chemistry libraries for drug discovery. 1. A qualitative and quantitative characterization of known drug databases. *J. Comb. Chem.* **1999**, *1*, 55–68.
- Walsh, G. *Pharmaceutical Biotechnology: Concepts and Applications*; 1<sup>st</sup> ed.; John Wiley & Sons: Nashville, TN, 2013.
- Khalid, H.; Aziz-ur-Rehman; Abbasi, M. A.; Malik, A.; Rasool, S.; Nafeesa, K.; Ahmad, I.; Afzal, S. Synthesis, spectral analysis and anti-bacterial study of *N*-substituted derivatives of 2-(5-(1-(phenylsulfonyl) piperidin-4-yl)-1,3,4-oxadiazol-2-ylthio)acetamide. *J. Saudi Chem. Soc.* **2016**, *20*, S615–S623.
- Autore, G.; Caruso, A.; Marzocco, S.; Nicolaus, B.; Palladino, C.; Pinto, A.; Popolo, A.; Sinicropi, M. S.; Tommonaro, G.; Saturnino, C. Acetamide derivatives with antioxidant activity and potential anti-inflammatory activity. *Molecules* **2010**, *15*, 2028–2038.
- Hazra, B.; Pore, V.; Dey, S.; Datta, S.; Darokar, M.; Saikia, D.; Khanuja, S. P. S.; Thakur, A. Bile acid amides derived from chiral amino alcohols: novel antimicrobials and antifungals. *Bioorg. Med. Chem. Lett.* **2004**, *14*, 773–777.
- Sawant, R.; Kawade, D. Synthesis and biological evaluation of some novel 2-phenyl benzimidazole-1-acetamide derivatives as potential anthelmintic agents. *Acta Pharm.* **2011**, *61*, 353–361.
- Hu, J.; Yu, M.; Yu, P.; Xu, Y. Synthesis and antimicrobial activity of novel benzisothiazolin-3-one acetamide derivatives. *Asian J. Chem.* **2014**, *26*, 7680–7682.
- Shridhar Deshpande, N.; Mahendra, G. S.; Aggarwal, N. N.; Gatphoh, B. F. D.; Revanasiddappa, B. C. In silico design, ADMET screening, MM-GBSA binding free energy of novel 1,3,4 oxadiazoles linked Schiff bases as PARP-1 inhibitors targeting breast cancer. *Futur. J. Pharm. Sci.* **2021**, *7*, 174.
- Daina, A.; Michielin, O.; Zoete, V. SwissADME: a free web tool to evaluate pharmacokinetics, drug-likeness and medicinal chemistry friendliness of small molecules. *Sci. Rep.* **2017**, *7*, 42717.
- Filimonov, D. A.; Lagunin, A. A.; Glorizova, T. A.; Rudik, A. V.; Druzhilovskii, D. S.; Pogodin, P. V.; Poroikov, V. V. Prediction of the biological activity spectra of organic compounds using the pass online web resource. *Chem. Heterocycl. Compd. (N. Y.)* **2014**, *50*, 444–457.
- Morris, G. M.; Huey, R.; Lindstrom, W.; Sanner, M. F.; Belew, R. K.; Goodsell, D. S.; Olson, A. J. AutoDock4 and AutoDockTools4: Automated docking with selective receptor flexibility. *J. Comput. Chem.* **2009**, *30*, 2785–2791.
- Karlberg, T.; Markova, N.; Johansson, I.; Hammarström, M.; Schütz, P.; Weigelt, J.; Schüler, H. Structural basis for the interaction between tankyrase-2 and a potent Wnt-signaling inhibitor. *J. Med. Chem.* **2010**, *53*, 5352–5355.
- Ryan, K.; Bolaños, B.; Smith, M.; Palde, P. B.; Cuenca, P. D.; VanArsdale, T. L.; Niessen, S.; Zhang, L.; Behenna, D.; Ornelas, M. A.; Tran, K. T.; Kaiser, S.; Lum, L.; Stewart, A.; Gajiwala, K. S. Dissecting the molecular determinants of clinical PARP1 inhibitor selectivity for tankyrase-1. *J. Biol. Chem.* **2021**, *296*, 100251.

- [15]. Yang, X.; Sun, R.; Zhang, C.; Zheng, X.; Yuan, M.; Fu, H.; Li, R.; Chen, H. Iridium-catalyzed benzylamine C-H alkenylation enabled by pentafluorobenzoyl as the directing group. *Org. Lett.* **2019**, *21*, 1002–1006.
- [16]. Mumtaz, A.; Mahmud, T.; Mr, E. Synthesis and characterization of new Schiff base transition metal complexes derived from drug together with biological potential study. *J. Nucl. Med. Radiat. Ther.* **2016**, *07*, 6.
- [17]. Narasimharao, K.; Chemistry Department, Faculty of Science, King Abdulaziz University, P.O. Box 80203, Jeddah 21589, Saudi Arabia Design, spectroscopic characterization, electrical conductivity and molecular modelling studies of biologically puissant Co(II) and Ni(II) complexes of N,N'-bis(furan-2-ylmethyl)benzene-1,2- dicarboxamide. *Int. J. Electrochem. Sci.* **2016**, *7*, 282–7307.
- [18]. Bruker (2015). APEX3. Bruker AXS Inc., Madison, Wisconsin, USA.
- [19]. Bruker (2008). SAINT. Bruker AXS Inc., Madison, Wisconsin, USA.
- [20]. Sheldrick, G. M. A short history of SHELX. *Acta Crystallogr. A* **2008**, *64*, 112–122.
- [21]. Spek, A. L. Structure validation in chemical crystallography. *Acta Crystallogr. D Biol. Crystallogr.* **2009**, *65*, 148–155.
- [22]. Dolomanov, O. V.; Bourhis, L. J.; Gildea, R. J.; Howard, J. A. K.; Puschmann, H. OLEX2: a complete structure solution, refinement and analysis program. *J. Appl. Crystallogr.* **2009**, *42*, 339–341.
- [23]. Farrugia, L. J. ORTEP-3 for Windows - a version of ORTEP-III with a Graphical User Interface (GUI). *J. Appl. Crystallogr.* **1997**, *30*, 565–565.
- [24]. Spackman, P. R.; Turner, M. J.; McKinnon, J. J.; Wolff, S. K.; Grimwood, D. J.; Jayatilaka, D.; Spackman, M. A. CrystalExplorer: a program for Hirshfeld surface analysis, visualization and quantitative analysis of molecular crystals. *J. Appl. Crystallogr.* **2021**, *54*, 1006–1011.
- [25]. Frisch, M. J.; Trucks, G. W.; Schlegel, H. B.; Scuseria, G. E.; Robb, M. A.; Cheeseman, J. R.; Montgomery, J. A.; Vreven, T.; Kudin, K. N.; Burant, J. C.; Millam, J. M.; Iyengar, S. S.; Tomasi, J.; Barone, V.; Mennucci, B.; Cossi, M.; Scalmani, G.; Rega, N.; Petersson, G. A.; Nakatsuji, H.; Hada, M.; Ehara, M.; Toyota, K.; Fukuda, R.; Hasegawa, J.; Ishida, M.; Nakajima, T.; Honda, Y.; Kitao, O.; Nakai, H.; Klene, M.; Li, X.; Knox, J. E.; Hratchian, H. P.; Cross, J. B.; Adamo, C.; Jaramillo, J.; Gomperts, R.; Stratmann, R. E.; Yazyev, O.; Austin, A. J.; Cammi, R.; Pomelli, C.; Ochterski, J. W.; Ayala, P. Y.; Morokuma, K.; Voth, G. A.; Salvador, P.; Dannenberg, J. J.; Zakrzewski, V. G.; Dapprich, S.; Daniels, A. D.; Strain, M. C.; Farkas, O.; Malick, D. K.; Rabuck, A. D.; Raghavachari, K.; Foresman, J. B.; Ortiz, J. V.; Cui, Q.; Baboul, A. G.; Clifford, S.; Cioslowski, J.; Stefanov, B. B.; Liu, G.; Liashenko, A.; Piskorz, P.; Komaromi, I.; Martin, R. L.; Fox, D. J.; Keith, T.; Al-Laham, M. A.; Peng, C. Y.; Nanayakkara, A.; Challacombe, M.; Gill, P. M. W.; Johnson, B.; Chen, W.; Wong, M. W.; Gonzalez, C.; Pople, J. A. Gaussian 09, rev. A.01, Gaussian, Inc., Wallingford CT, 2013.
- [26]. Bhabha, G.; Ekiert, D. C.; Jennewein, M.; Zmasek, C. M.; Tuttle, L. M.; Kroon, G.; Dyson, H. J.; Godzik, A.; Wilson, I. A.; Wright, P. E. Divergent evolution of protein conformational dynamics in dihydrofolate reductase. *Nat. Struct. Mol. Biol.* **2013**, *20*, 1243–1249.
- [27]. Blanco, B.; Prado, V.; Lence, E.; Otero, J. M.; Garcia-Doval, C.; van Raaij, M. J.; Llamas-Saiz, A. L.; Lamb, H.; Hawkins, A. R.; González-Bello, C. Mycobacterium tuberculosis shikimate kinase inhibitors: Design and simulation studies of the catalytic turnover. *J. Am. Chem. Soc.* **2013**, *135*, 12366–12376.
- [28]. Ritchie, T. J.; Ertl, P.; Lewis, R. The graphical representation of ADME-related molecule properties for medicinal chemists. *Drug Discov. Today* **2011**, *16*, 65–72.
- [29]. Dunnett, C. W. New tables for multiple comparisons with a control. *Biometrics* **1964**, *20*, 482–491.
- [30]. Tung, N.; Garber, J. E. PARP inhibition in breast cancer: progress made and future hopes. *NPJ Breast Cancer* **2022**, *8*, 47.
- [31]. Qiu, W.; Lam, R.; Voytyuk, O.; Romanov, V.; Gordon, R.; Gebremeskel, S.; Vodsedalek, J.; Thompson, C.; Beletskaya, I.; Battaile, K. P.; Pai, E. F.; Rottapel, R.; Chirgadze, N. Y. Insights into the binding of PARP inhibitors to the catalytic domain of human tankyrase-2. *Acta Crystallogr. D Biol. Crystallogr.* **2014**, *70*, 2740–2753.
- [32]. DeLano, W. L. The PyMOL Molecular Graphics System DeLano Scientific: San Carlos, CA, 2002. <https://www.pymol.org> (accessed August 10, 2022).
- [33]. Wallace, A. C.; Laskowski, R. A.; Thornton, J. M. LIGPLOT: a program to generate schematic diagrams of protein-ligand interactions. *Protein Eng. Des. Sel.* **1995**, *8*, 127–134.
- [34]. Schöning-Stierand, K.; Diedrich, K.; Fährrolfes, R.; Flachsenberg, F.; Meyder, A.; Nittinger, E.; Steinegger, R.; Rarey, M. ProteinsPlus: interactive analysis of protein-ligand binding interfaces. *Nucleic Acids Res.* **2020**, *48*, W48–W53.
- [35]. Stierand, K.; Maass, P. C.; Rarey, M. Molecular complexes at a glance: automated generation of two-dimensional complex diagrams. *Bioinformatics* **2006**, *22*, 1710–1716.
- [36]. Kansiz, S.; Çakmak, S.; Dege, N.; Meral, G.; Kütük, H. Crystal Structure of 3-Acetoxy-2-methyl-N-(4-nitrophenyl)benzamide. *X-ray Struct. Anal. Online* **2018**, *34*, 17–18.
- [37]. Mackenzie, C. F.; Spackman, P. R.; Jayatilaka, D.; Spackman, M. A. CrystalExplorer model energies and energy frameworks: extension to metal coordination compounds, organic salts, solvates and open-shell systems. *IUCr* **2017**, *4*, 575–587.
- [38]. Abbaz, T.; Bendjedou, A.; Villemin, D. Molecular structure, HOMO, LUMO, MEP, natural bond orbital analysis of benzo and anthra quinodimethane derivatives. *Pharm. Biol. Evaluations* **2018**, *5*, 27–39.
- [39]. Uzun, S.; Esen, Z.; Koç, E.; Usta, N. C.; Ceylan, M. Experimental and density functional theory (MEP, FMO, NLO, Fukui functions) and antibacterial activity studies on 2-amino-4-(4-nitrophenyl)-5,6-dihydrobenzo[h]quinoline-3-carbonitrile. *J. Mol. Struct.* **2019**, *1178*, 450–457.
- [40]. Cortesi, L.; Rugo, H. S.; Jackisch, C. An overview of PARP inhibitors for the treatment of breast cancer. *Target. Oncol.* **2021**, *16*, 255–282.
- [41]. Griguolo, G.; Dieci, M. V.; Guarneri, V.; Conte, P. Olaparib for the treatment of breast cancer. *Expert Rev. Anticancer Ther.* **2018**, *18*, 519–530.
- [42]. Litton, J. K.; Rugo, H. S.; Ettl, J.; Hurvitz, S. A.; Gonçalves, A.; Lee, K.-H.; Fehrenbacher, L.; Yerushalmi, R.; Mina, L. A.; Martin, M.; Roché, H.; Im, Y.-H.; Quek, R. G. W.; Markova, D.; Tudor, I. C.; Hannah, A. L.; Eiermann, W.; Blum, J. L. Talazoparib in patients with advanced breast cancer and a germline BRCA mutation. *N. Engl. J. Med.* **2018**, *379*, 753–763.



Copyright © 2022 by Authors. This work is published and licensed by Atlanta Publishing House LLC, Atlanta, GA, USA. The full terms of this license are available at <http://www.eurjchem.com/index.php/eurjchem/pages/view/terms> and incorporate the Creative Commons Attribution-Non Commercial (CC BY NC) (International, v4.0) License (<http://creativecommons.org/licenses/by-nc/4.0>). By accessing the work, you hereby accept the Terms. This is an open access article distributed under the terms and conditions of the CC BY NC License, which permits unrestricted non-commercial use, distribution, and reproduction in any medium, provided the original work is properly cited without any further permission from Atlanta Publishing House LLC (European Journal of Chemistry). No use, distribution or reproduction is permitted which does not comply with these terms. Permissions for commercial use of this work beyond the scope of the License (<http://www.eurjchem.com/index.php/eurjchem/pages/view/terms>) are administered by Atlanta Publishing House LLC (European Journal of Chemistry).